

WHITE DWARFS IN THE CALÁN-ESO SURVEY¹

MARIA TERESA RUIZ²

Departamento de Astronomía, Universidad de Chile, Casilla 36-D, Santiago, Chile; mtruiz@das.uchile.cl

AND

P. BERGERON

Département de Physique, Université de Montréal, C.P. 6128, Succursale Centre-Ville, Montréal, Québec H3C 3J7, Canada; bergeron@astro.umontreal.ca

Received 2001 March 26; accepted 2001 May 11

ABSTRACT

A sample of 33 white dwarfs (31 of them previously unknown) was recently discovered as a result of a proper-motion survey using red plates, which covered 350 deg² in the sky. In this paper we present spectroscopic and photometric observations for all objects. The sample contains 15 non-DA white dwarfs (including several DQ and DZ stars) and 17 DA white dwarfs (including one DAZ star). One other object (CE 315) is an interacting double-degenerate and has been analyzed elsewhere. Atmospheric compositions, effective temperatures, and cooling ages have been estimated using model atmosphere fits to the observed fluxes. One white dwarf, CE 51, with a hydrogen-rich atmosphere, has a preliminary temperature estimate of only $T_{\text{eff}} = 2730$ K, the coolest white dwarf identified so far in the literature. Atmospheric parameters for some DA stars in the sample have also been derived from fits to the high Balmer line profiles. From the present sample, a lower limit to the density of white dwarfs in the solar neighborhood, $\rho = 5.6 \times 10^{-3}$ pc⁻³, has been derived.

Subject headings: astrometry — white dwarfs — surveys

On-line material: machine-readable tables

1. INTRODUCTION

During the last 12 years, a proper-motion survey was carried out using red IIIa-F plates, taken with the Schmidt Camera at La Silla (Ruiz et al. 2001b). The search covered 350 deg² in the sky, down to $m_R \sim 19.5$, resulting in a catalog of 542 stars with $\mu \geq 0''.20$ yr⁻¹. The spectroscopic follow-up of faint high proper-motion stars in the Calán-ESO (CE) survey revealed the presence of several new white dwarfs, some of them cool (dim) enough to be considered “dark matter.” Coordinates and finding charts for these objects are given in Ruiz et al. (2001b). Out of 24 white dwarfs found in the CE Catalog, CE 16 and CE 51 are both Luyten half-second (LHS) objects (Luyten 1979; the finding chart for CE 51 in the LHS atlas points to the wrong object, however) and three white dwarfs are Luyten two-tenths (LTT) objects (CE 85, CE 86, and CE 117), while CE 354 (WD 1338-311, ESO 445-271), CE 356 (WD 1340-308, ESO 445-249), and CE 421 (WD 1411-363, ESO 385-268) have previously been reported by Ruiz (1996) and analyzed by Bergeron, Ruiz, & Leggett (1997).

Nine common proper-motion binary systems were found. Four of them have proper motions of $\geq 0''.20$ yr⁻¹, and are therefore in the CE catalog. Three of these binaries are double degenerates: CE 315, an unresolved, interacting double degenerate that has been analyzed elsewhere (Ruiz et al. 2001a), CE 85 and CE 86, which are a known system included in the white dwarf catalog by McCook & Sion (1999) with numbers 0935-37.2 and 0935-37.1, respectively, and the binary of ESO 496-512 and ESO 496-513. Tables 1 and 2 provide astrometric and photometric data for both

components of the common proper-motion systems found (except for CE 315).

Here we present spectroscopic and photometric observations of all the white dwarfs in the CE catalog, and model atmosphere fits are used to determine the effective temperature, atmospheric composition, and stellar age of each object. We also report and analyze nine white dwarfs with $\mu \lesssim 0''.2$ yr⁻¹, found in a nonsystematic way during the survey (most turned out to be members of common proper-motion binary systems). However, in this case, the sample is by no means complete. Finding charts for these non-CE objects are provided in Figure 1, and their astrometric data are given in Table 1, which also includes the main-sequence companions to the white dwarfs in common proper-motion systems.

2. OBSERVATIONS

The follow-up spectroscopy of proper-motion stars in the Calán-ESO survey has been obtained over the last eight years using the Cerro Tololo Inter-American Observatory (CTIO) Blanco telescope and the ESO 3.6 m telescope at La Silla.

The Blanco telescope was equipped with the Ritchey-Chrétien spectrograph and a Loral 3K detector using grating KPGL3. This combination produced spectra covering the range between 3800 and 7000 Å, with a resolution of 4 Å. Stars CE 16, CE 40, CE 50/51, CE 85/86, CE 117, CE 142, CE 157, CE 273, CE 296, CE 315, CE 421, CE 532/533, CE 108, ESO 384-48/49, ESO 496-512/513, ESO 496-290/291, and ESO 496-358/359 were observed with this setup. Spectroscopy for the rest of the stars, namely CE 162, CE 233, CE 270, CE 282, CE 315 (this star was observed with both telescopes), CE 349, CE 354, CE 356, CE 452, CE 510, CE 514, ESO 381-186, ESO 445-316/317, ESO 508-151, and ESO 508-162, was obtained at the ESO 3.6 m telescope with the ESO faint-object spectrograph and camera (EFOSC 2)

¹ This paper is based on observations obtained at La Silla (ESO), Chile. Project 64.H-0318.

² Visiting Astronomer, Cerro Tololo Inter-American Observatory, NOAO, which is operated by AURA Inc., under cooperative agreement with the National Science Foundation.

TABLE 1
 WHITE DWARFS IN THE SURVEY WITH $\mu \lesssim 0.2 \text{ yr}^{-1}$, AND THEIR COMMON PROPER
 MOTION COMPANIONS

Name	α (2000)	δ (2000)	ST	μ (arcsec yr ⁻¹)	θ (deg)
ESO 496-290.....	8 43 55.8	-25 20 38.9	DZ	0.12	329.7
ESO 496-291.....	8 43 55.8	-25 20 46.3	M3.7	0.12	329.7
ESO 496-512.....	8 55 50.7	-26 37 45.3	DA	0.13	201.1
ESO 496-513.....	8 55 51.1	-26 37 50.3	DA	0.13	201.1
ESO 496-358.....	8 56 41.2	-25 48 46.4	M4.6	0.04	1.6
ESO 496-359.....	8 56 41.5	-25 48 44.8	DA	0.04	1.6
ESO 381-186.....	13 01 55.5	-34 25 29.4	DA	0.12	246.4
ESO 508-151.....	13 12 07.4	-25 54 24.3	DAZ	0.03	38.3
ESO 508-162.....	13 16 15.6	-26 04 46.7	DA	0.06	230.7
ESO 445-316.....	13 43 26.4	-31 51 29.9	M4.8	0.16	260.6
ESO 445-317.....	13 43 27.5	-31 51 30.7	DA	0.16	260.6
ESO 384-48.....	13 59 08.7	-33 10 30.3	M4.0	0.16	213.7
ESO 384-49.....	13 59 09.2	-33 10 47.2	DA	0.16	213.7

NOTE.—Units of right ascension are hours, minutes, and seconds, and units of declination are degrees, arcminutes, and arcseconds.

and the B300b grism, which produced spectra with a resolution of 12 Å, ranging from 3700 to 7100 Å. In each case, the slit was rotated to the parallactic angle to avoid loss of light due to atmospheric refraction. In order to calibrate the flux and wavelength of the spectra, four spectrophotometric standards were observed during each night, and a He-Ar lamp calibration was taken at the beginning of the night. The data were reduced using IRAF.

In all plots, the region below 3900 Å has been cut off because of very poor flat-field correction at shorter wavelengths, where there is very little signal from the flat-field lamps, and most of the counts come from stray light originating from internal reflections (which also affects the data themselves).

The spectra for all DA (hydrogen line) white dwarfs in the sample are displayed in Figure 2, in order of decreasing effective temperature. ESO 508-151 represents a new

member of the DAZ spectral class (hydrogen line spectrum with metallic lines visible; see Zuckerman & Reid 1998, and references therein), with the Ca II H and K lines clearly visible near 4000 Å.

The spectra for all non-DA white dwarfs in the sample are displayed in Figure 3, in order of decreasing effective temperature. From this plot, CE 51 already appears to be significantly cooler than the remaining white dwarfs in the sample. Most objects in Figure 3 have featureless spectra (DC stars), although some clearly show the C₂ Swan band at 5165 Å and are thus DQ stars (CE 85, CE 273, and CE 349), while others are DZ stars with detectable Ca II H and K lines (CE 349, CE 354, and ESO 496-290). Note that CE 349 is a unique object, with carbon bands and metallic lines simultaneously present in the spectrum, together with what appears to be a CH molecular band near 4400 Å, similar to that observed in G99-37 (Wesemael et al. 1993). This is

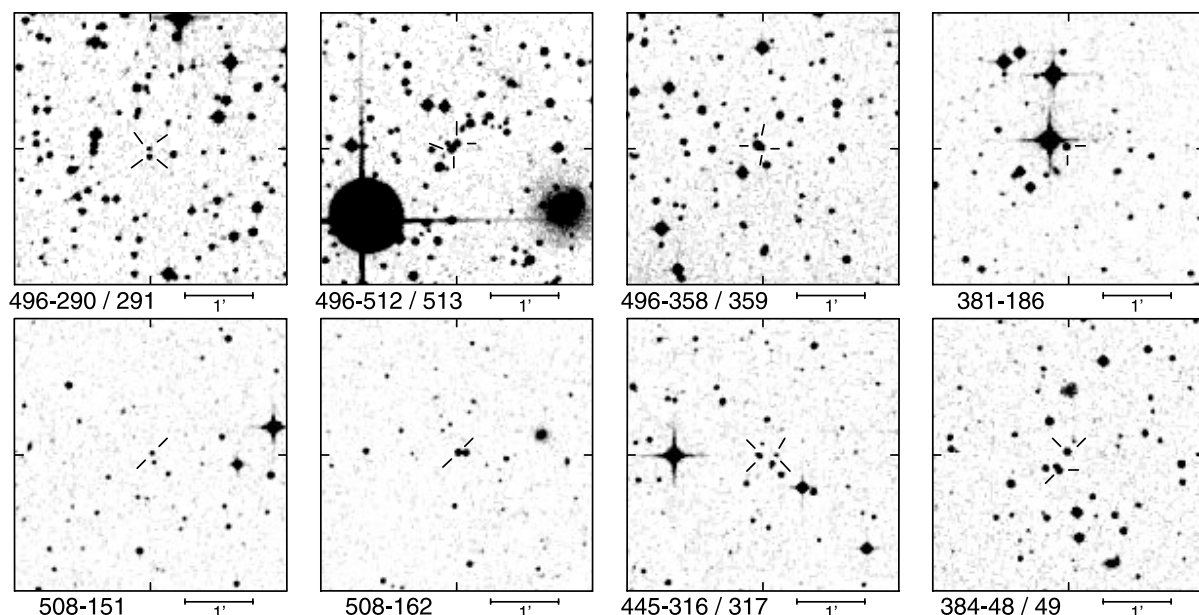


FIG. 1.—Charts extracted from the Digitized Sky Survey, each covering an area of $4' \times 4'$. North is up and east is to the left.

TABLE 2
OBSERVATIONAL RESULTS

Name	W (Å)	ST	V	$B-V$	$V-R$	$V-I$
CE 16.....	0.0	DC	18.35	+1.42	+0.76	+1.41
CE 40.....	0.0	DC	19.48	+1.23	+0.66	+1.25
CE 50.....	...	M5.8	18.04	+2.02	+1.74	+3.94
CE 51.....	0.0	DC	18.07	+1.77	+0.57	+0.76
CE 85.....	0.0	DQ	14.83	+0.09	+0.10	+0.19
CE 86.....	12.2	DA	15.20	+0.23	+0.17	+0.37
CE 108.....	10.9	DA	16.77	+0.30	+0.22	+0.46
CE 117.....	29.1	DA	15.45	+0.03	-0.06	-0.10
CE 142.....	0.0	DC	19.32	+1.36	+0.73	+1.39
CE 157.....	8.9	DA	15.89	+0.36	+0.25	+0.53
CE 162.....	4.7	DA	17.05	+0.57	+0.36	+0.81
CE 233.....	2.8	DA	18.74	+0.74	+0.38	+0.78
CE 270.....	0.0	DC	19.66	+0.89	+0.45	+0.98
CE 273.....	0.0	DQ	14.62	+0.12	+0.12	+0.22
CE 282.....	0.0	DC	19.54	+1.30	+0.62	+1.24
CE 296.....	0.0	DQ	15.77	+0.20	+0.16	+0.31
CE 315.....	0.0	DD	17.67	-0.44	+0.20	+0.40
CE 349.....	0.0	DQZ	19.16	+0.59	+0.22	+0.40
CE 354.....	0.0	DZ	17.25	+0.17	+0.14	+0.29
CE 356.....	8.4	DA	16.89	+0.48	+0.32	+0.71
CE 421.....	1.0	DA	17.86	+0.90	+0.51	+0.98
CE 452.....	0.0	DC	19.25	+1.20	+0.62	+1.17
CE 510.....	15.3	DA	19.19	+0.29	+0.25	+0.40
CE 514.....	0.0	DC	16.16	+0.41	+0.31	+0.60
CE 532.....	...	M4.5	17.76	+1.68	+1.35	+3.14
CE 533.....	0.0	DC	19.04	+0.66	+0.43	+0.80
ESO 496-290...	0.0	DZ	19.83	+0.51	+0.11	+0.33
ESO 496-291...	...	M3.7	18.32	+1.58	+1.20	+2.74
ESO 496-512...	12.9	DA	16.83	+0.25	+0.16	+0.36
ESO 496-513...	16.0	DA	16.97	+0.21	+0.13	+0.30
ESO 496-358...	...	M4.6	17.44	+1.55	+1.39	+3.20
ESO 496-359...	40.4	DA	16.51	+0.11	-0.05	-0.03
ESO 381-186...	32.5	DA	17.37	+0.13	+0.00	-0.03
ESO 508-151...	3.4	DAZ	19.19	+0.51	+0.29	+0.69
ESO 508-162...	14.3	DA	17.25	-0.10	-0.08	-0.10
ESO 445-316...	...	M4.8	19.08	+2.05	+1.52	+3.39
ESO 445-317...	11.5	DA	18.18	+0.39	+0.25	+0.47
ESO 384-48....	...	M4.0	16.27	+1.64	+1.26	+2.88
ESO 384-49....	4.7	DA	17.68	+0.49	+0.31	+0.62

NOTE.—Table 2 is also available in machine-readable form in the electronic edition of the *Astrophysical Journal*.

illustrated in Figure 4, where the spectrum of CE 349 is plotted together with that of a DZ white dwarf (CE 354) and the DQ white dwarf G99-37.

Optical *BVRI* photometry for the stars in this sample was obtained using the CTIO 1.5 and 0.9 m telescopes during several observing runs. The accuracy is typically $\sim 2\%$, and in a few cases it could be as much as $\sim 4\%$. Results are summarized in Table 2, where we also include the spectral type (ST) for each object. For each white dwarf in the sample, we also provide the measured $H\alpha$ equivalent width (W); an equivalent width of zero implies that the spectrum is featureless near the $H\alpha$ region.

3. RESULTS

3.1. Model Atmosphere Analysis

The energy distribution for each white dwarf has been obtained by converting the observed magnitudes into broadband fluxes, following Bergeron et al. (1997). These energy distributions are then fitted with those predicted

from the model atmospheres of Bergeron, Saumon, & Wesemael (1995), using a nonlinear least-squares method (see Bergeron et al. 1997 for details). Only T_{eff} and the solid angle $(R/D)^2$, where R is the radius of the star and D its distance from Earth, are considered free parameters. Given that these white dwarfs have no trigonometric parallax measurements, a value of $\log g = 8.0$ has been assumed for all objects. As discussed in Bergeron et al. (1997), the B magnitude of hydrogen-rich white dwarfs with a temperature below $T_{\text{eff}} \sim 5500$ K is affected by a UV flux deficiency, most likely related to a pseudocontinuum opacity originating from the Lyman edge, and it was thus omitted in the fits of the cooler hydrogen-rich white dwarfs. CE 315 has been excluded from the analysis, since this object was found to be an interacting double-degenerate star with an emission line spectrum dominated by He lines; a complete analysis of this system has been presented by Ruiz et al. (2001a).

The analysis of Bergeron et al. (1997; see also Bergeron, Leggett, & Ruiz 2001) has stressed the importance of using infrared photometry for analyzing cool white dwarf stars. In particular, the infrared H - and K -bandpasses represent the most important discriminant between hydrogen-rich and helium-rich energy distributions. Unfortunately, our photometric observations lack this crucial information. Nonetheless, we are still able to determine in most cases whether the atmosphere is hydrogen rich or helium rich using *BVRI* photometry combined with spectroscopy at $H\alpha$, although our temperature scale may still be affected by the lack of infrared photometric measurements.

Results of the model fits to the energy distributions are summarized in Table 3. For each white dwarf, we give (always assuming $\log g = 8.0$ for each object) the effective temperature, the dominant atmospheric constituent, the predicted absolute visual magnitude, the total luminosity, the white dwarf cooling age (not including the main-sequence lifetime), the distance, and the measured tangential velocity. We have assumed pure hydrogen and pure helium compositions for the hydrogen- and helium-rich white dwarfs, respectively. The error for T_{eff} is derived directly from the fits to the energy distributions, and it is propagated to the other quantities. The C/O core evolutionary models with thin and thick hydrogen layers, described in Bergeron et al. (2001) based on the calculations of Fontaine, Brassard, & Bergeron (2001), have been used for the helium- and hydrogen-dominated atmospheres, respectively.

Illustrative fits for hydrogen-rich white dwarf stars in our sample are presented in Figure 5. The observed fluxes are represented by error bars, while the fluxes predicted by the models are shown as filled circles. The atmospheric parameters of each fit are given in the left panels. In the right panels, the spectroscopic observations near the $H\alpha$ region are shown, together with theoretical line profiles interpolated at the value of T_{eff} obtained from the energy distribution fits (again assuming $\log g = 8.0$). A good fit to the observed $H\alpha$ line profile constitutes an independent check of the derived atmospheric parameters.

CE 51 (member of a common proper-motion system with CE 50), with a temperature of only 2730 K, represents by far the coolest white dwarf star yet identified in the literature. Infrared photometric measurements are required, however, before a more reliable temperature estimate can be obtained. A more complete analysis of this object will be

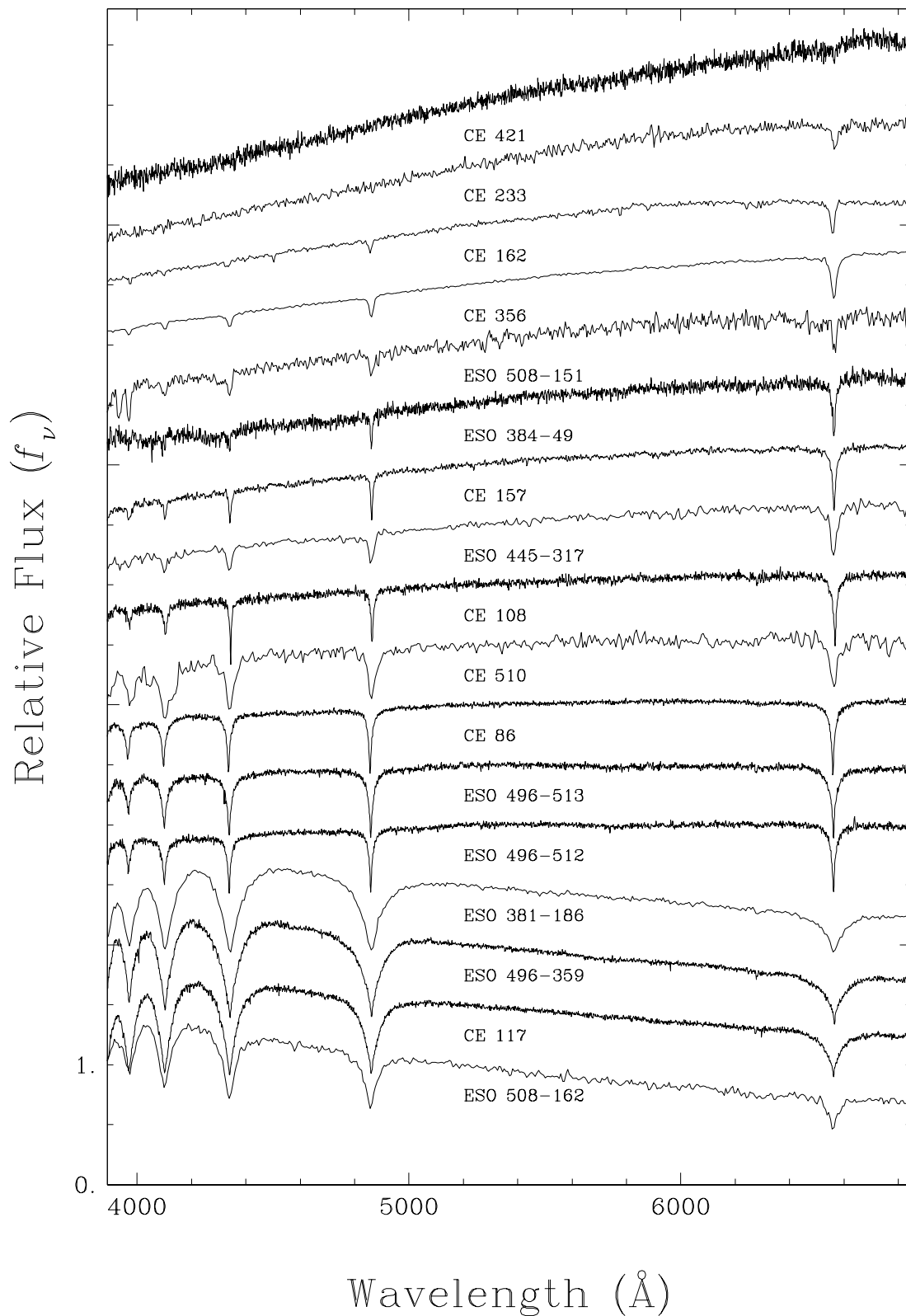


FIG. 2.—Optical spectra for the complete sample of DA white dwarfs. The spectra are normalized at 5200 \AA , and are shifted vertically from each other by 0.5. The effective temperature increases from top to bottom.

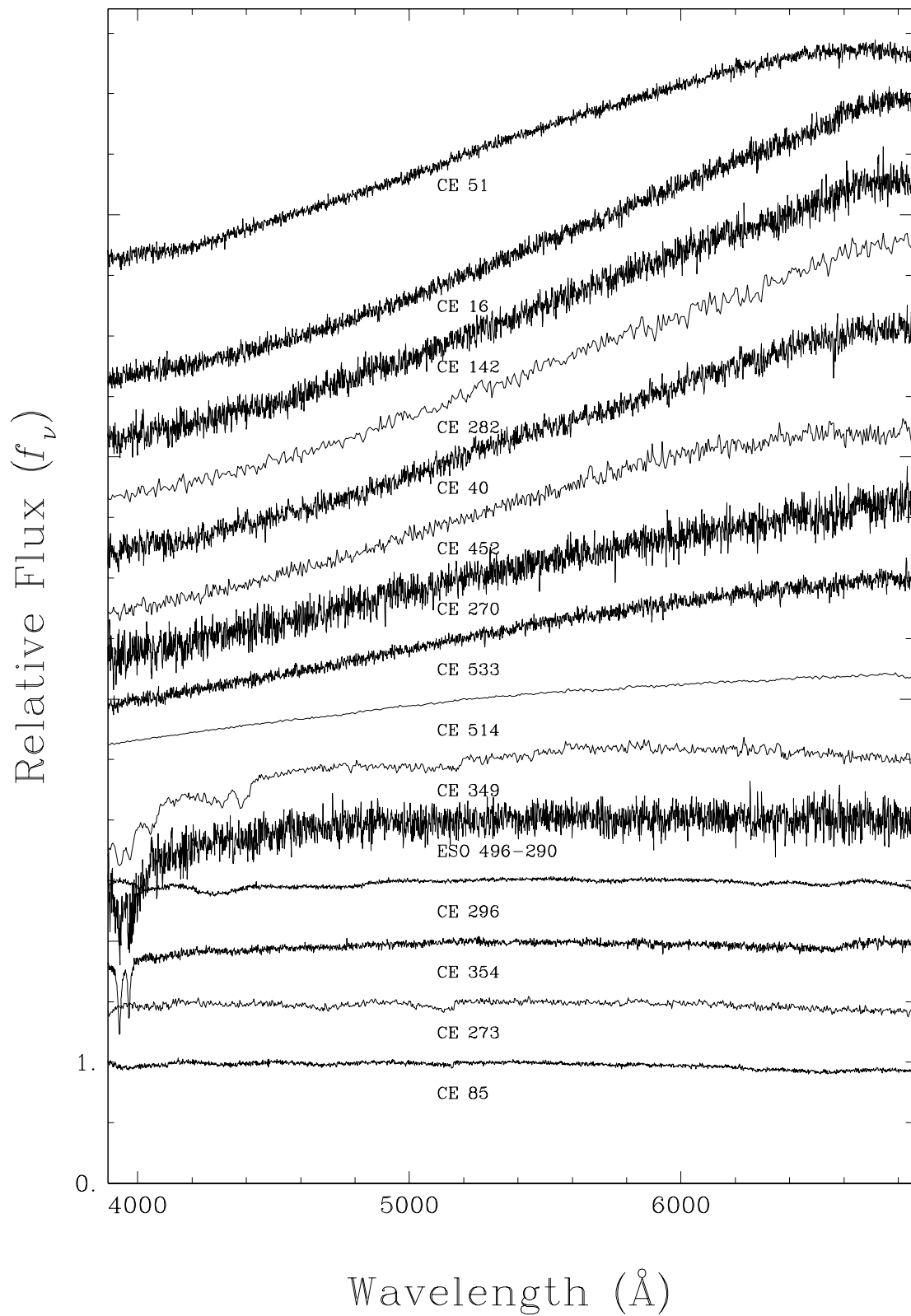


FIG. 3.—Same as Fig. 2, except for showing the complete sample of non-DA white dwarfs

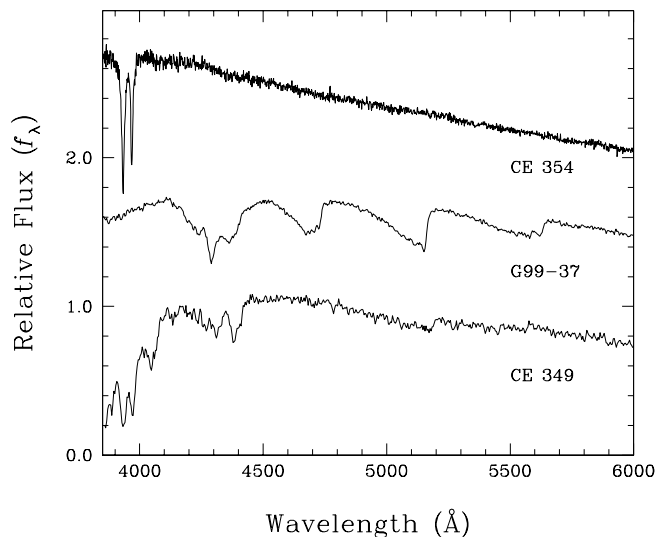


FIG. 4.—Comparison of the spectrum of CE 349 with those of a DZ white dwarf (CE 354) and a DQ white dwarf showing a CH feature (G99-37). The spectra are normalized at 4800 Å, and are shifted vertically from each other by 0.7.

reported elsewhere. Other ultracool white dwarfs with temperature estimates include LHS 3250 (Harris et al. 1999; $T_{\text{eff}} \sim 2000\text{--}4000$ K), F351-50 (Ibata et al. 2000; Oppenheimer et al. 2001b; $T_{\text{eff}} \sim 3500$ K), WD 0346+246

(Oppenheimer et al. 2001b; $T_{\text{eff}} = 3750$ K), and SDSS 1337+00 (Harris et al. 2001; $T_{\text{eff}} \sim 3000\text{--}4000$ K). Additional cool white dwarf candidates have also been identified by Oppenheimer et al. (2001a), although no detailed analysis of these objects has been performed yet.

In Figure 6 we present illustrative fits for non-DA white dwarfs. This time, the panels on the right show the observed (featureless) spectra near the H α region, together with the theoretical profile predicted under the assumption of a hydrogen-rich atmosphere. This simply illustrates the expected strength of H α at this temperature if the star has a hydrogen-rich atmosphere. Pure helium atmosphere white dwarfs are of course featureless at these temperatures.

Our spectroscopic observations of the hottest DA stars in the sample also include the high Balmer line series (see Fig. 2), which allows us to use the spectroscopic technique to obtain independent estimates of T_{eff} and $\log g$. The first step is to normalize the line flux, in both observed and model spectra, to a continuum set to unity. The comparison with model spectra, which are convolved with the appropriate Gaussian instrumental profile, is then carried out only in terms of these normalized line profiles. Here we consider only H β to H8 in the fitting procedure. The results for all DA stars with strong enough Balmer lines are reported in Table 4, in which the stellar mass and absolute visual magnitude have been determined using the thick-hydrogen-layer models described above. Illustrative fits at various effective temperatures are displayed in Figure 7.

TABLE 3

ATMOSPHERIC PARAMETERS DETERMINED FROM PHOTOMETRY

Name	T_{eff} (K)	Composition	M_V	$\log L/L_{\odot}$	Age (Gyr)	D (pc)	V_T (km s $^{-1}$)
CE 16.....	4330 \pm 30	He	16.10 \pm 0.05	−4.31	7.57	28.2 \pm 0.7	79
CE 40.....	4580 \pm 30	He	15.67 \pm 0.05	−4.21	6.99	57.9 \pm 1.4	125
CE 51.....	2730 \pm 30	H	17.23 \pm 0.05	−5.10	11.86	14.7 \pm 0.3	68
CE 85.....	10050 \pm 340	He	12.27 \pm 0.09	−2.83	0.65	32.5 \pm 1.4	30
CE 86.....	8240 \pm 240	H	12.92 \pm 0.11	−3.17	1.00	28.6 \pm 1.4	30
CE 108.....	7490 \pm 190	H	13.29 \pm 0.09	−3.34	1.28	49.7 \pm 2.1	26
CE 117.....	15440 \pm 860	H	11.21 \pm 0.10	−2.06	0.18	70.3 \pm 3.1	53
CE 142.....	4390 \pm 30	He	16.00 \pm 0.05	−4.28	7.43	46.2 \pm 1.2	72
CE 157.....	7000 \pm 160	H	13.55 \pm 0.09	−3.45	1.52	29.4 \pm 1.2	38
CE 162.....	5730 \pm 100	H	14.43 \pm 0.08	−3.81	2.61	33.5 \pm 1.2	15
CE 233.....	5410 \pm 90	H	14.65 \pm 0.08	−3.91	3.53	65.6 \pm 2.4	44
CE 270.....	5120 \pm 40	He	14.93 \pm 0.05	−4.01	5.59	88.4 \pm 2.1	63
CE 273.....	9610 \pm 310	He	12.40 \pm 0.09	−2.91	0.73	27.7 \pm 1.2	16
CE 282.....	4540 \pm 30	He	15.69 \pm 0.05	−4.22	7.07	58.8 \pm 1.4	70
CE 296.....	8560 \pm 250	He	12.77 \pm 0.10	−3.11	0.99	39.9 \pm 1.8	48
CE 349.....	7570 \pm 360	He	13.20 \pm 0.15	−3.33	1.36	155.8 \pm 11.2	124
CE 354.....	8870 \pm 270	He	12.65 \pm 0.09	−3.05	0.91	83.1 \pm 3.7	61
CE 356.....	6160 \pm 110	H	14.09 \pm 0.08	−3.68	2.09	36.3 \pm 1.3	21
CE 421.....	4760 \pm 70	H	15.36 \pm 0.08	−4.13	6.69	31.7 \pm 1.2	21
CE 452.....	4660 \pm 30	He	15.52 \pm 0.05	−4.18	6.81	55.7 \pm 1.3	30
CE 510.....	7730 \pm 200	H	13.16 \pm 0.10	−3.28	1.18	160.3 \pm 7.2	148
CE 514.....	6520 \pm 130	He	13.80 \pm 0.08	−3.59	1.97	29.7 \pm 1.0	99
CE 533.....	5580 \pm 70	He	14.49 \pm 0.06	−3.86	3.67	81.4 \pm 2.2	93
ESO 496-290.....	8130 \pm 430	He	12.91 \pm 0.17	−3.20	1.14	242.5 \pm 18.6	132
ESO 496-512.....	8210 \pm 240	H	12.92 \pm 0.11	−3.18	1.00	60.5 \pm 3.0	21
ESO 496-513.....	8760 \pm 270	H	12.68 \pm 0.11	−3.06	0.85	72.2 \pm 3.8	21
ESO 496-359.....	12920 \pm 670	H	11.53 \pm 0.08	−2.38	0.31	99.1 \pm 3.8	32
ESO 381-186.....	12340 \pm 680	H	11.61 \pm 0.08	−2.46	0.35	142.0 \pm 5.3	55
ESO 508-151.....	6150 \pm 110	H	14.07 \pm 0.08	−3.68	2.10	105.5 \pm 3.8	38
ESO 508-162.....	19190 \pm 990	H	10.86 \pm 0.13	−1.68	0.08	189.8 \pm 11.2	27
ESO 445-317.....	7080 \pm 160	H	13.48 \pm 0.08	−3.43	1.48	87.0 \pm 3.5	43
ESO 384-49.....	6330 \pm 120	H	13.95 \pm 0.08	−3.63	1.95	55.7 \pm 1.9	21

NOTE.—Table 3 is also available in machine-readable form in the electronic edition of the *Astrophysical Journal*.

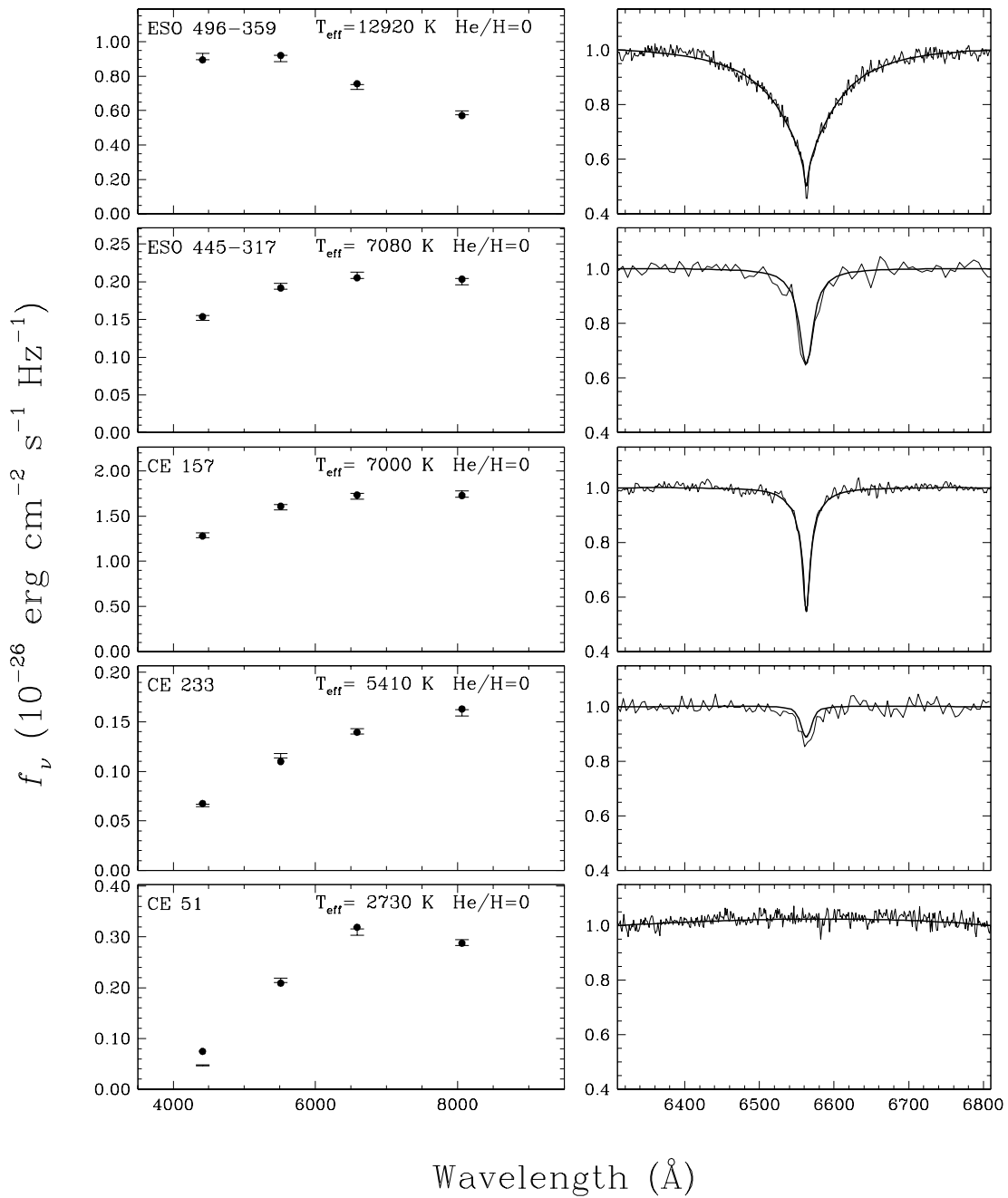


FIG. 5.—Fits to the energy distributions of hydrogen-rich stars with pure hydrogen atmosphere models. The *BVRI* photometric observations are represented by error bars, while the model fluxes are shown as filled circles. In the right panels are shown the observed normalized spectra together with the synthetic line profiles interpolated at the parameters obtained from the energy distribution fits in the left panels.

In general, the agreement between the photometrically derived parameters and those obtained from the Balmer line profiles are very consistent, as can be seen from Figure 8, in which we have plotted the T_{eff} derived from both methods. Exceptions include ESO 508-162 ($\Delta T_{\text{eff}} \sim 7000$ K; not seen in Figure 8), for which the spectroscopic temperature is preferred, given the lack of sensitivity of *BVRI* photometry near 20,000 K, and CE 117, which has a surface gravity of $\log g = 7.42$ ($M = 0.34 M_{\odot}$), which implies that the object is most likely a double-degenerate binary.

3.2. Space Density of White Dwarfs

There has been a long-standing controversy regarding

the number density of white dwarfs in our Galaxy. Liebert, Dahn, & Monet (1988) derived a space density of $\rho = 3.3 \times 10^{-3} \text{ pc}^{-3}$, while predictions based on the star formation history of our Galaxy (Twarog 1980; Noh & Scalo 1990) and those based on theory (D’Antona & Mazzitelli 1989) suggest a much larger number density (10 to 100 times larger), with ages ~ 9 Gyr. Other more recent determinations of the number density of white dwarfs (Oswalt et al. 1996; Knox, Hawkins, & Hambly 1999; Tat & Terzian 1999) have derived values that are clearly larger than the original value found by Liebert et al. (1988).

The present sample has been identified from a survey with well-understood limits (Ruiz et al. 2001b). Therefore, one can attempt to obtain the number density of white

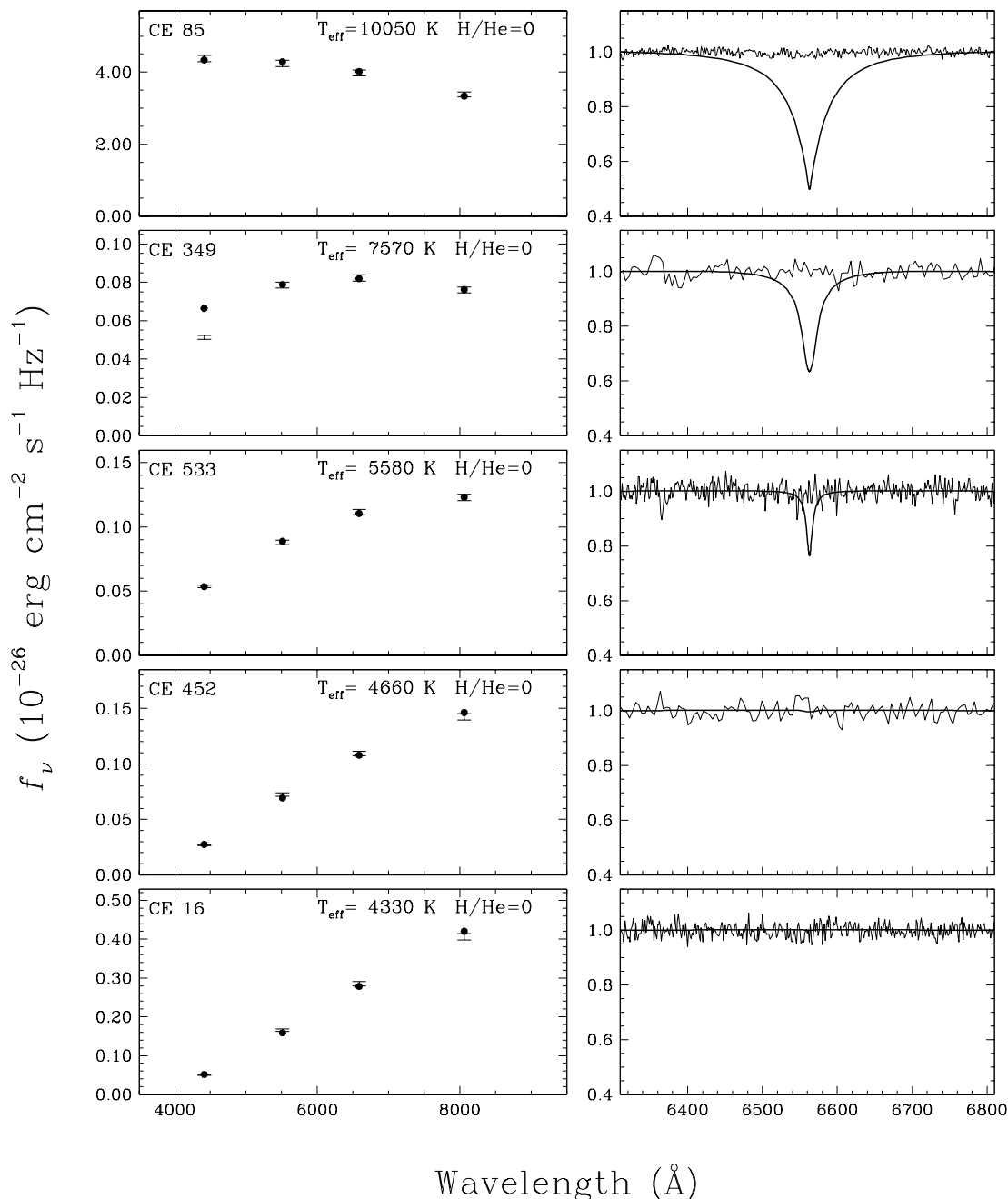


FIG. 6.—Fits to the energy distributions of helium-rich stars with pure helium atmosphere models. The *BVRI* photometric observations are represented by error bars, while the model fluxes are shown as filled circles. In the right panels are shown the observed normalized spectra together with the synthetic line profiles calculated with the parameters obtained from the energy distribution fits in the left panels, but assuming a pure hydrogen atmosphere composition.

dwarfs using distances derived from the model atmosphere analysis discussed above and given in Table 3.

In the 350 deg² of sky covered by the CE survey (14 ESO areas of 25 deg² each), we should have found all the white dwarfs within 37 pc; beyond that distance, the faintest white dwarfs would have apparent magnitudes fainter than the magnitude limit of the survey. The CE survey, based on red IIIa-F plates taken with the ESO Schmidt Camera, has a magnitude limit of $m_R \sim 19.5$. The completeness analysis of the CE catalog (Ruiz et al. 2001b) indicates that the catalog is complete down to $\mu = 0.2 \text{ yr}^{-1}$.

On the other hand, the faintest white dwarf known so far is ESO 439-26 (Ruiz et al. 1995), with an absolute magni-

tude in R of $M_R = 16.76$, which is very close to the $M_R = 16.66$ of CE 51, the faintest white dwarf in this sample. Assuming that CE 51 represents the intrinsically faintest white dwarf that can exist, we should have found all the white dwarfs out to a distance of 37 pc, corresponding to a volume of 1800 pc³. From Table 3, we can see that there are 10 CE white dwarfs in such a volume. Assuming that there is a uniform distribution of white dwarfs in space, one should find half that amount (five objects) in the nearest 900 pc³, that is, with distances smaller than ~ 30 pc. In Table 3 we find six stars with $D \lesssim 30$ pc, confirming our initial assumption that we have found all the white dwarfs up to a distance of 37 pc. There is a huge loss of white dwarfs for

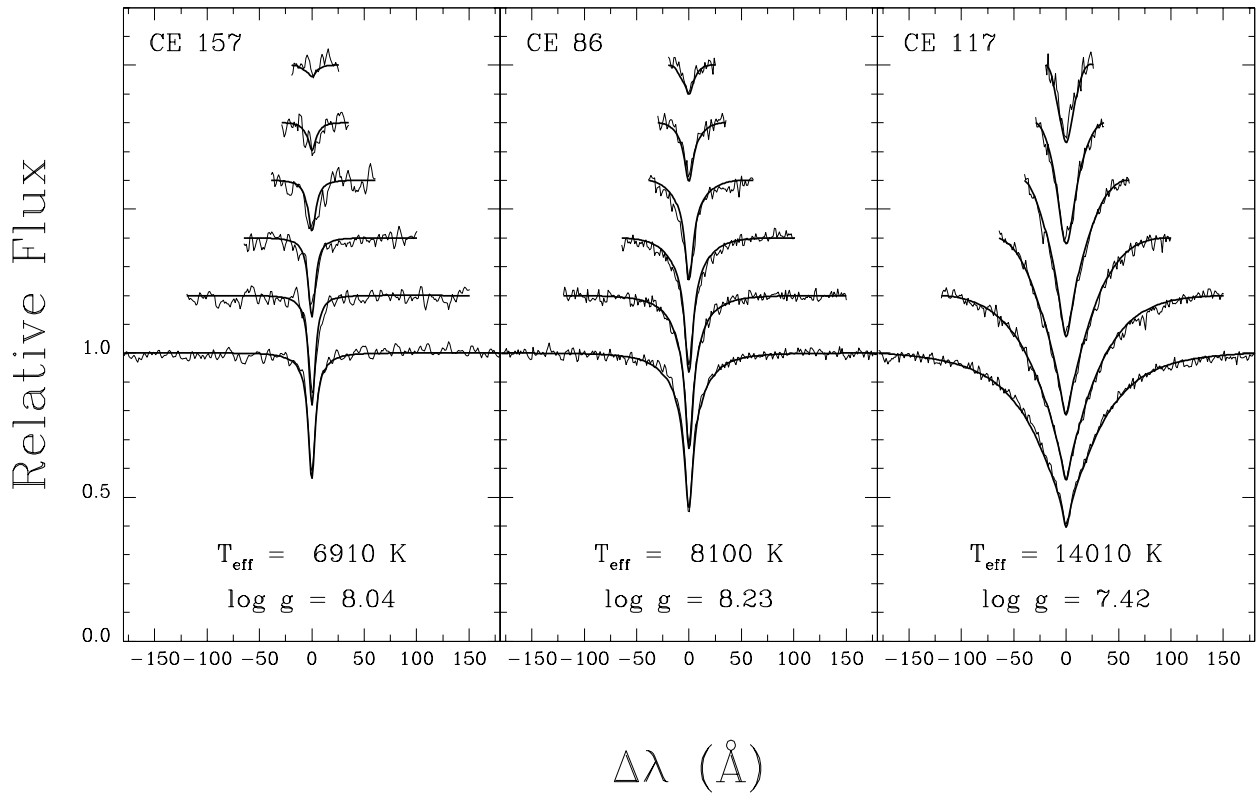


FIG. 7.—Illustrative fits to the individual Balmer line profiles for three DA stars in our sample. The lines range from H β (bottom) to H9 (top), each offset vertically by a factor of 0.2.

larger distances, where we are severely affected by the magnitude limit of the survey. For example, in a volume of 3600 pc³, corresponding to a distance of 47 pc, there should be 20 white dwarfs, and we only find 12.

As a consequence, we derive a white dwarf space density of $\rho = 5.6 \times 10^{-3}$ pc⁻³, which is almost twice the density determined by Liebert et al. (1988). On the other hand, the space density determined here is affected by the kinematical bias introduced by selecting stars based only on their proper motions. White dwarfs with most of their motion along the radial component will not be found by our survey. Therefore, the space density of white dwarfs determined above should be considered a lower limit. The density found

above is in remarkable agreement with the density $\rho = 5.54 \times 10^{-3}$ pc⁻³ found by Holberg, Oswalt, & Sion (2001), counting all the known white dwarfs within 13 pc from the Sun (51 white dwarfs).

TABLE 4

ATMOSPHERIC PARAMETERS DETERMINED FROM SPECTROSCOPY

Name	T_{eff} (K)	log g	M/M_{\odot}	M_V
CE 86.....	8100 ± 22	8.23 ± 0.03	0.738 ± 0.02	13.30
CE 108.....	7350 ± 44	8.36 ± 0.07	0.820 ± 0.05	13.89
CE 117.....	14010 ± 102	7.42 ± 0.02	0.344 ± 0.01	10.55
CE 157.....	6910 ± 38	8.04 ± 0.07	0.616 ± 0.04	13.65
CE 356.....	6550 ± 81	8.36 ± 0.17	0.824 ± 0.11	14.35
ESO 496-512...	8930 ± 28	8.36 ± 0.04	0.825 ± 0.03	13.55
ESO 496-513...	8700 ± 28	8.64 ± 0.04	1.007 ± 0.02	13.74
ESO 496-359...	13680 ± 215	7.93 ± 0.02	0.570 ± 0.01	11.30
ESO 381-186...	13230 ± 658	7.82 ± 0.06	0.509 ± 0.03	11.21
ESO 508-162...	26090 ± 333	7.98 ± 0.05	0.624 ± 0.03	10.19
ESO 445-317...	7090 ± 132	8.43 ± 0.25	0.868 ± 0.16	14.14

NOTE.—Table 4 is also available in machine-readable form in the electronic edition of the *Astrophysical Journal*.

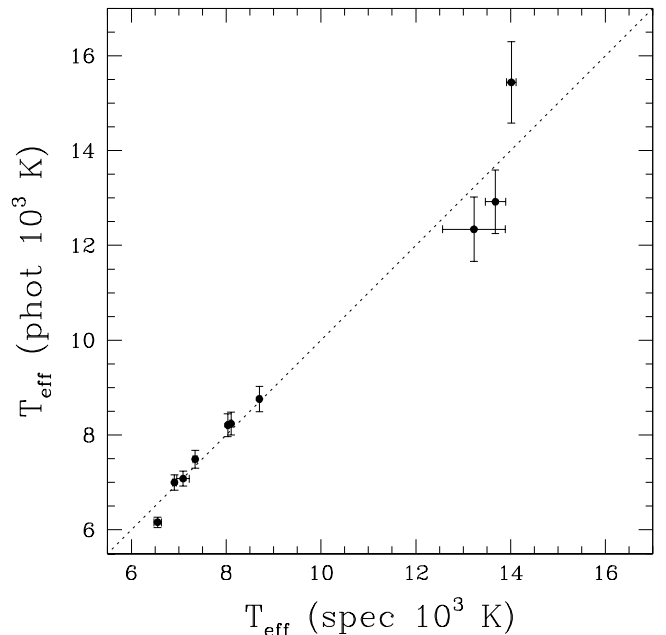


FIG. 8.—Comparison of the effective temperatures determined from the photometric technique (*phot*) and from the spectroscopic technique (*spec*) for all DA stars in our sample with strong enough Balmer lines. The dashed line indicates the 1:1 correspondence. ESO 508-162 with $T_{\text{eff}}(\text{phot}) = 19,190$ K and $T_{\text{eff}}(\text{spec}) = 26,090$ K lie outside the figure.

M. T. R. received partial support from FONDECYT grant 1980659 and Catedra Presidencial en Ciencias. This work was supported in part by the NSERC Canada and by the Fund FCAR (Québec). The Digitized Sky Surveys were produced at the Space Telescope Science Institute under US Government grant NAG W-2166. The images of these

surveys are based on photographic data obtained using the Oschin Schmidt Telescope at Palomar Mountain and the UK Schmidt Telescope. The plates were processed into their current compressed digital form with the permission of these institutions.

REFERENCES

- Bergeron, P., Leggett, S. K., & Ruiz, M. T. 2001, *ApJS*, 133, 413
 Bergeron, P., Ruiz, M. T., & Leggett, S. K. 1997, *ApJS*, 108, 339
 Bergeron, P., Saumon, D., & Wesemael, F. 1995, *ApJ*, 443, 764
 D'Antona, F., & Mazzitelli, I. 1989, *ApJ*, 347, 934
 Fontaine, G., Brassard, P., & Bergeron, P. 2001, *PASP*, 113, 409
 Harris, H. C., Dahn, C. C., Vrba, F. J., Henden, A. A., Liebert, J., Schmidt, G. D., & Reid, I. N. 1999, *ApJ*, 524, 1000
 Harris, H. C., et al. 2001, *ApJ*, 549, L109
 Holberg, J. B., Oswalt, T. D., & Sion, E. M. 2001, preprint (astro-ph/0102120)
 Ibata, R., Irwin, M., Bienaymé, O., Scholz, R., & Guibert, J. 2000, *ApJ*, 532, L41
 Knox, R. A., Hawkins, M. R. S., & Hambly, N. C. 1999, *MNRAS*, 306, 736
 Liebert, J., Dahn, C., & Monet, D. G. 1988, *ApJ*, 332, 891
 Luyten, W. J. 1979, *The LHS Catalogue* (2d ed.; Minneapolis: Univ. of Minnesota)
 McCook, G. P., & Sion, E. M. 1999, *ApJS*, 121, 1
 Noh, H. R., & Scalo, J. 1990, *ApJ*, 352, 605
 Oppenheimer, B. R., Hambly, N. C., Digby, A. P., Hodgkin, S. T., & Saumon, D. 2001a, *Science*, 292, 698
 Oppenheimer, B. R., Saumon, D., Hodgkin, S. T., Jameson, R. F., Hambly, N. C., Chabrier, G., Filipenko, A. V., Coil, A. L., & Brown, M. E. 2001b, *ApJ*, 550, 448
 Oswalt, T. D., Smith, J. A., Wood, M. A., Hintzen, P. 1996, *Nature*, 382, 692
 Ruiz, M. T. 1996, *AJ*, 111, 1267
 Ruiz, M. T., Bergeron, P., Leggett, S. K., & Anguita, C. 1995, *ApJ*, 455, L159
 Ruiz, M. T., Rojo, P. M., Garay, G., & Maza J. 2001a, *ApJ*, 552, 679
 Ruiz, M. T., Wischnjewsky, M., Rojo, P., & Gonzalez, L. E. 2001b, *ApJS*, 133, 119
 Tat, H. H., & Terzian, Y. 1999, *PASP*, 111, 1258
 Twarog, B. A. 1980, *ApJ*, 242, 242
 Wesemael, F., Greenstein, J. L., Liebert, J., Lamontagne, R., Fontaine, G., Bergeron, P., & Glaspey, J. W. 1993, *PASP*, 105, 761
 Zuckerman, B., & Reid, I. N. 1998, *ApJ*, 505, L143